

Article

Structural and Luminescent Peculiarities of Spark Plasma Sintered Transparent MgAl_2O_4 Spinel Ceramics Doped with Cerium Ions

Damir Valiev *, Sergey Stepanov , Vladimir Paygin , Oleg Khasanov, Edgar Dvilis and Lin Chaolu

School of Advanced Manufacturing Technologies, National Research Tomsk Polytechnic University, Lenin Avenue 30, Tomsk 634050, Russia

* Correspondence: rubinf@tpu.ru

Abstract: In the present study, the concentration series of $\text{MgAl}_2\text{O}_4:\text{Ce}^{3+}$ ceramics have been fabricated by the Spark Plasma Sintering (SPS) method. Cerium-doping concentration was varied within a range of 0.1–5 wt.%. The prepared ceramics have been tested using the various experimental techniques: X-ray diffraction (XRD), scanning electron microscopy, as well as optical and cathodoluminescence spectroscopy. According to XRD, all synthesized samples are biphasic with structural impurities. The cerium ion concentration effect on the cathodoluminescent characteristics of $\text{MgAl}_2\text{O}_4:\text{Ce}^{3+}$ ceramics has been studied in terms of emission intensity and decay time. Before annealing the concentration, quenching is observed. The optimal doping Ce^{3+} concentration was determined to be 5 wt.% after temperature annealing at 1300 °C. The successfully prepared spinel ceramics could be potentially applying for high-energy electrons detection.

Keywords: MgAl_2O_4 spinel ceramics; cerium ions; SPS technique; optical properties; cathodoluminescence



Citation: Valiev, D.; Stepanov, S.; Paygin, V.; Khasanov, O.; Dvilis, E.; Chaolu, L. Structural and Luminescent Peculiarities of Spark Plasma Sintered Transparent MgAl_2O_4 Spinel Ceramics Doped with Cerium Ions. *Inorganics* **2022**, *10*, 153. <https://doi.org/10.3390/inorganics10100153>

Academic Editor: Sergey Kuznetsov

Received: 29 July 2022

Accepted: 21 September 2022

Published: 26 September 2022

Publisher's Note: MDPI stays neutral with regard to jurisdictional claims in published maps and institutional affiliations.



Copyright: © 2022 by the authors. Licensee MDPI, Basel, Switzerland. This article is an open access article distributed under the terms and conditions of the Creative Commons Attribution (CC BY) license (<https://creativecommons.org/licenses/by/4.0/>).

1. Introduction

Transparent MgAl_2O_4 ceramics is one of the most promising oxide optical materials [1–6]. Spinel ceramics can be used as elements of “active” optics, such as active laser media, dosimeters etc. [7,8]. High values of the transmittance of electromagnetic radiation in a wide spectral range from 200 nm to 5500 nm without optical distortion and non-hygroscopic properties make the spinel material promising for use in scintillators and converters of ionizing radiation [9,10]. Moreover, transparent MgAl_2O_4 are used in aviation and space technology [11,12]. It is used to produce elements of optical telescopes, passive optics, output windows of ultraviolet and infrared laser devices operating in extreme conditions [13,14].

Sintering of spinel ceramics can be implemented using various technological approaches, such as low-temperature sintering, hot pressing (HP) [15,16], hot isostatic pressing (HIP) [17,18], and Spark Plasma Sintering (SPS) [19–21]. In recent years, the SPS method has been widely used to consolidate powders of various types of materials. The main reason is that, compared with well-known HP or HIP technologies, high heating rates, exceeding 50 °C/min, can reduce the total processing time when compacting the powder. In the SPS process, a uniform distribution of density in the volume of sintered ceramics occurs relative to traditional manufacturing methods, and perfect-grain boundaries are formed [19,22].

The development of scientifically substantiated methods for the synthesis of the oxide ceramics with controlled optical and luminescent properties, in combination with the necessary physical and mechanical characteristics, is an urgent problem. To control the physical and chemical properties of ceramics, fundamental knowledge of the electronic excitations' dynamics features in the ceramic hosts of various compositions is required. The luminescent properties of ceramics directly depend on the defect structure of the material,

which includes oxygen vacancies and impurity ions. Rare earth (RE) ions are traditionally used as a dopant [23–27]. It should be noted that the problem of low solubility of dopants in spinel, which leads to the formation of secondary phases and degradation of optical properties. The indicated problem can be solved by using nanodispersed powders as starting materials, which have a higher effectiveness compared to microdispersed analogs. The effective methods of mixing and consolidation procedure can be also applied [28–30].

There are several papers devoted to the study of MgAl_2O_4 transparent ceramics [31,32]. However, at the same time, there are no systematic studies aimed at obtaining MgAl_2O_4 -ceramics doped with RE ions fabricated by the SPS method and the analysis of their luminescent properties. RE ions are used as sintering additives in the manufacture of MgAl_2O_4 ceramics. At present, studies of MgAl_2O_4 nanopowders doped with RE ions are being actively carried out [33–39]. The possibility of obtaining transparent luminescent MgAl_2O_4 ceramics doped with Yb_2O_3 was demonstrated in ref. [40] and doped with CeO_2 in refs. [41–43]. The authors of [41] consider MgAl_2O_4 as a promising material for scintillation applications. The low stopping power of the spinel can be compensated by the greater thickness of the scintillation material plates or used in combined detectors.

Previously, we demonstrated the possibility of obtaining transparent luminescent MgAl_2O_4 ceramics doped with europium, cerium oxide [42,43], terbium oxide, and dysprosium [44] with a concentration level of 0.1 wt.%. However, there is a need to conduct research on optimizing the SPS technology of consolidating ceramics with higher levels of RE ions' doping. However, there is a need to conduct research on spinel ceramics with high levels of dopant concentrations. In the present work, we studied the effect of cerium ions on structural, optical and luminescent properties of MgAl_2O_4 ceramics fabricated by the SPS method.

2. Results and Discussion

2.1. Powders Characterization

A scanning electron microscopy (SEM) image of a commercial aluminum magnesium spinel nanopowder SC30R is shown in Figure 1a. Primary particles of the initial nanopowders had a shape close to spherical with average sizes from 26 nm to 269 nm. The powder consisted of both primary particles and agglomerates ranging in size from tens to several hundreds of nanometers. According to laser diffraction data, the structural elements of the aluminum-magnesium spinel powder range in size from 10 nm to 2.9 μm . The particle-size distribution of the powder is shown in Figure 1c. The BET surface area was $24.9 \text{ m}^2 \cdot \text{g}^{-1}$ and corresponded to a particle diameter of 67 nm (in the spherical approximation) (Figure 1b). The discrepancies between the data on the average particle size obtained using different methods were due to the deviation from the spherical particle shape and agglomeration of the primary powder particles. This was confirmed by the SEM results.

A scanning transmission electron microscopy (STEM) image of commercial cerium oxide nanopowders is shown in Figure 1c. The powder consisted of separate non-equiaxed particles with an average size of 25 nm. There were no particle agglomerates in the obtained transmission electron microscopy (TEM) image. The size of the powder structural elements varied from 10 nm to 220 nm according to laser diffraction data (Figure 1d). The average size of the structural elements was 64 nm. The BET surface area of the investigated nanopowders was $11.59 \text{ m}^2 \cdot \text{g}^{-1}$, corresponding to a diameter of 73 nm.

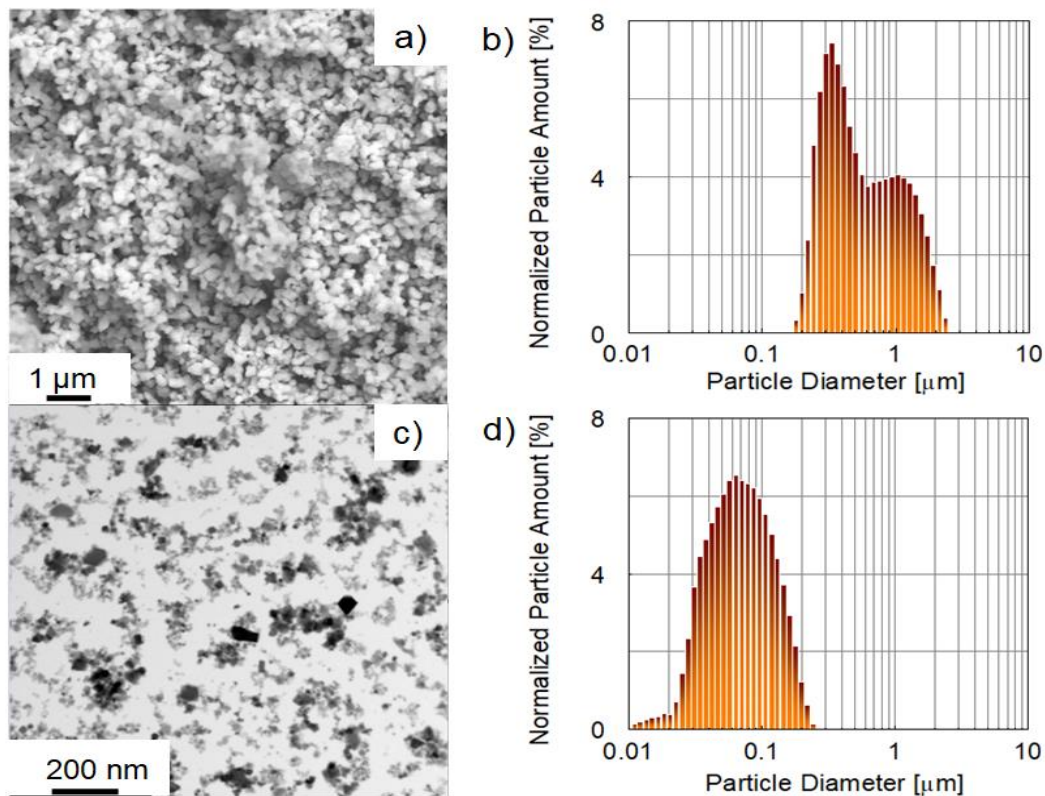


Figure 1. SEM (a), scanning transmission electron microscopy (STEM) (c) images, and particle size distributions (b,d) of MgAl_2O_4 and CeO_2 nanopowders.

2.2. Ceramics Characterization

The linear-shrinkage dynamics of $\text{MgAl}_2\text{O}_4\text{:Ce}$ ceramics during the SPS process is presented in Figure 2a. An analysis of the obtained dependencies made it possible to establish that the main part of shrinkage fell on the nonisothermal heating stage. Shrinkage curves of sintered ceramics were single-stage in nature. Thermal shrinkage under pressure started at temperatures between 985 °C and 1025 °C. High shrinkage intensity was observed in the temperature range from 985 °C to 1100 °C. At this stage, there was a decrease in porosity, consolidation, and grain growth. In the temperature range from 1100 °C to 1245 °C, the shrinkage intensity slowed down significantly and practically stopped when the temperature reached 1300 °C at the stage of isothermal exposure. The introduction of 0.1 wt.% cerium oxide nanopowders in the MgAl_2O_4 host spinel did not have a significant effect on the SPS process (Figure 2a). Temperature deviations did not fall outside the confidence interval for measuring this value (± 50 °C). There was a shift in the interval of intense shrinkage to the temperature range from 1100 °C to 1285 °C when the cerium oxide concentrations increased from 0.1 wt.% to 1 wt.%. A further increase in the concentration of cerium oxide up to 5 wt.%, also led to a shift in the shrinkage range to higher temperatures. The shrinkage process slowed down at a temperature of 1300 °C during isothermal exposure and did not stop until it ended.

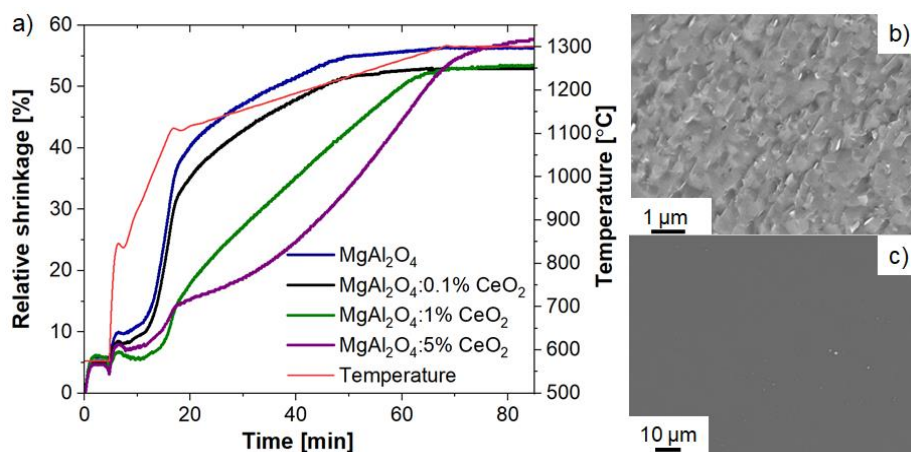


Figure 2. Linear shrinkage dynamics of undoped and Ce-doped MgAl₂O₄ ceramics during the SPS consolidating process (a). SEM images of fabricated ceramics analyzed from fracture (b) and surface (c) side, respectively.

An analysis of the structural morphology in the MgAl₂O₄:Ce samples based on the SEM results of the cleavage surface revealed a predominantly transcrystalline fracture pattern. It indicated a high strength and quality of grain boundaries of ceramics (Figure 2b). The average ceramic grain size remained in the submicron range, about 850 nm. The grain boundary size did not exceed 1 nm. Grains of another phase possibly corresponding to the Ce-dopant were found that can be clearly seen from SEM images obtained in the phase contrast mode. Their number increased with increasing cerium oxide content (Figure 2c).

The results of X-ray phase analysis of MgAl₂O₄:Ce samples are presented in Figure 3a. Two phases were observed in spinel ceramics: the alumina-magnesium spinel phase and the CeO₂ compound (PDF #000-21-1152). There was a 4 to 10-fold increase in the size of the coherent scattering region (CSR) as a result of sintering compared with the initial MgAl₂O₄ powder. The average CSR sizes with an increase in the CeO₂ concentration from 0 wt.% to 5 wt.% changed from 187 nm to 364 nm. The crystal lattice microstrains varied in a range from 0.000106 to 0.000176. The smallest value of CSR and the largest microstrains value of the crystal lattice could be seen in MgAl₂O₄: 5 wt.% Ce ceramics (Figure 3b–d).

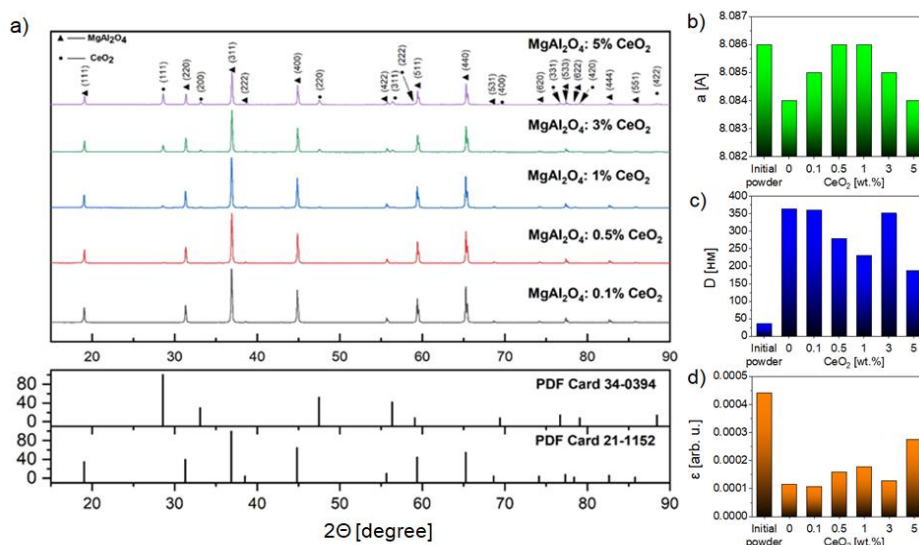


Figure 3. X-ray diffraction patterns (a) and the calculated crystal lattice parameters (b–d) of MgAl₂O₄: xCeO₂ ceramics.

2.3. Optical and Luminescent Properties

The in-line transmission spectra of undoped and MgAl₂O₄ ceramics doped with variable concentration of Ce ions before annealing are shown in Figure 4a,b, respectively.

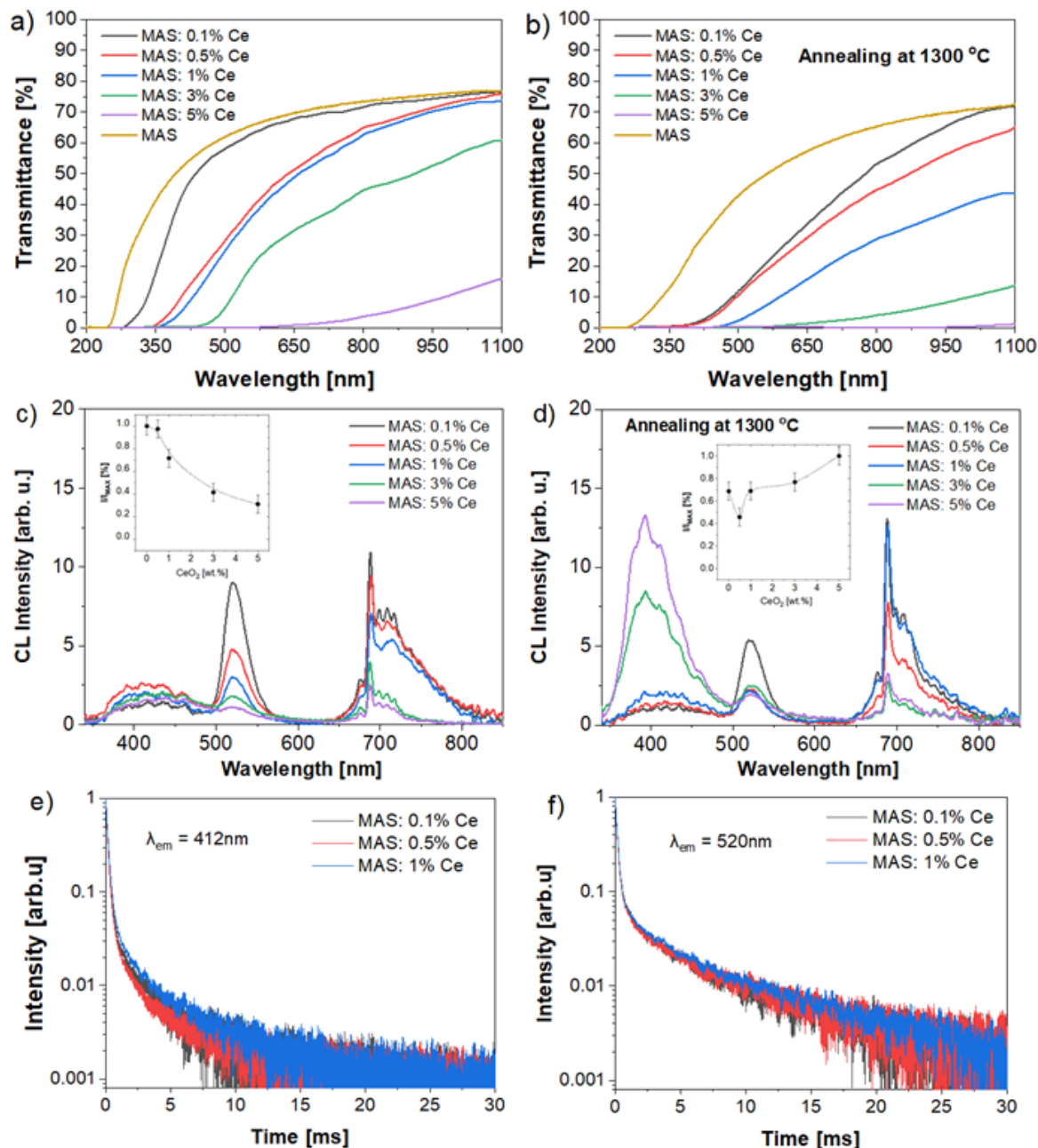


Figure 4. In-line transmittance spectra (a,b), cathodoluminescence spectra (c,d), and luminescence decay kinetics (e,f) of MgAl₂O₄:*x*Ce ceramics before and after annealing, respectively.

The transmittance for all samples decreased with an increase in the cerium ions concentration from 70% for 0.1% Ce in the visible and near-IR spectral ranges, respectively. The absorption edge wavelength for MgAl₂O₄:0.1% Ce ceramics was about 260 nm. The absorption edge of Ce-doped MgAl₂O₄ ceramics was shifted to the long wavelength spectral region and the effect of a red shift of the absorption edge was observed. The transmission edge in MgAl₂O₄:5% Ce ceramics was shifted to the spectral region of 600 nm. The transmittance was ~10% in the spectral range 600–1100 nm. The shape and edge of the transmission bands changed significantly after temperature annealing at 1300 °C. The absorption edge was

shifted to the spectral region of 350 nm for all ceramics samples. The transmittance values in the visible spectral range decreased for a wavelength of 500 nm to 10%. The transmittance value in the IR spectral range was consistent with the $\text{MgAl}_2\text{O}_4: x\text{Ce}$ ceramics samples before annealing and reduces with increasing cerium ion concentrations.

Several emission bands with peaks at 405, 520, and 688 nm were observed upon electron beam excitation of $\text{MgAl}_2\text{O}_4:\text{Ce}$ ceramics samples (Figure 4c,d). The emission band position was in good agreement with Refs. [25–28]. The emission band with a maximum at 405 nm was due to the radiative $4f \rightarrow 5d$ transition in the cerium ions. The charge-transfer transition could be described by the following mechanism. The Ce^{4+} was reduced to the excited state of Ce^{3+} , then the formed holes were captured by hole traps, and finally the excited state of Ce^{3+} ions passed into the ground state, emitting the photons at 405 nm. The broad luminescence band near 520 nm could be attributed to the V_k^{3+} luminescence center. When the ceramic was excited by the electron flow the Ce^{3+} ionized to form Ce^{4+} and excited the electrons transfer into the conduction band. At the end of the excitation process the electrons in the conduction band returned, were captured, and combined with holes in the V_k^{3+} center. This type of center would emit the photons with a wavelength of 520 nm. The luminescent properties of spinel ceramics before annealing were characterized by a decrease in the emission intensity of the bands at 412, 520, and 688 nm, respectively when the concentration of cerium ions increased (Figure 4b).

The opposite effect was observed with an increase in the cerium ions concentrations and an increase in the intensity of the luminescence band at 405 nm was recorded after annealing at a temperature of 1300 °C (Figure 4c). A possible reason for this effect may be that, at a high doping concentration, cerium cannot be incorporated into the spinel lattice, but retains the CeO_2 structure with the mixed phase formation. This led to the appearance of a large number of Ce^{4+} ions in $\text{MgAl}_2\text{O}_4:\text{Ce}$ ceramics. We can assume that the main luminescence mechanism was the reduction of Ce^{4+} to Ce^{3+} ions with a luminescence band at a wavelength of 405 nm. The emission band at 520 nm, on the contrary, demonstrated a tendency to decrease in intensity with an increase in the cerium ions concentration. This may be because the number of Ce^{4+} ions gradually increased with increasing doping concentration, which led to the transfer of the luminescence center. The emission band at 688 nm was associated with the radiation transitions in the Cr^{3+} impurity ions.

A study of the integral intensity of cathodoluminescence before annealing (Figure 4c, inset) showed that, when the cerium concentration increased from 0.1 to 5 wt.% the concentration of luminescence quenching was observed. After atmospheric annealing at a temperature of 1300 °C, the character of the dependence changed (Figure 4d, inset). A change in the cerium concentration from 0.1 to 0.5 wt% led to a reduction in the integrated luminescence intensity by 20%. For a cerium concentration of 1%, the integrated luminescence intensity was observed similar to a concentration of 0.1 wt%. An increase in the cerium concentration to 3 wt.% and 5 wt.% led to an enhancement in the luminescence intensity by 5% and 25%, respectively.

The luminescence decay kinetics in the millisecond time range were studied in three spectral regions: in the region of the “intrinsic” radiation at 412 nm; in the spectral region at 520 nm (Figure 4e,f). It was shown that the luminescence decay kinetics in the spectral regions consisted of several components with different lifetimes of the excited states. The luminescence decay kinetics were complex in character and could be approximated by the sum of three exponential functions as “fast” ($\tau_1 = 0.19 \pm 0.02$ ms) and “slow” ($\tau_2 = 4.6 \pm 0.5$ ms, $\tau_3 = 11 \pm 2$ ms). For an emission band at 699 nm associated with the chromium ion, the luminescence decay kinetic characteristics were also measured, but we did not find any differences in decay time. The same results were demonstrated in [42].

3. Materials and Methods

3.1. MgAl_2O_4 Ceramics Preparation

For the undoped and Ce-doped transparent MgAl_2O_4 ceramics fabrication the commercial aluminum magnesium spinel nanopowders (Baikowski Malakoff Inc., Malakoff,

TX, USA) and cerium oxide nanopowders (Merck KGaA, Darmstadt, Germany) was used. The mass measurement of the initial powders for the powder mixtures preparation and grinding bodies was carried out using a laboratory analytical balance Shinko AJ-420CE (Tokyo, Japan) with an accuracy of 0.001 g. Mixing and dispersion of the powders was carried out by the wet method using a ball mill for 48 h. The ratio of grinding media to powder was 5:1, respectively. The homogenous powders mixture was dried in a muffle furnace at 70 °C until moisture had completely evaporated. The series of $\text{MgAl}_2\text{O}_4:x\text{CeO}_2$ ($x = 0.1; 0.5; 1; 3; 5$ wt.%) ceramics were successfully fabricated.

Spinel ceramics were consolidated by the SPS method using an SPS-515S technological setup (Syntex Inc., Kawasaki, Japan) at a temperature of 1300 °C. The graphite die of uniaxial double-sided pressing with cylindrical cavity and punches was used for ceramics consolidation. The sintering process was carried out in vacuum at a residual pressure of not more than 10^{-3} Pa. The duration of isothermal exposure at a given sintering temperature was 20 min. The pressure throughout the entire sintering process was 100 MPa. The selection of the consolidation parameters was based on the results obtained earlier in [42,44]. Temperature control during the sintering process was estimated by a high-temperature optical pyrometer. Finally, cylindrical ceramics specimens were obtained at a size of 1.5–2 mm high and 14 mm in diameter. Ceramics were sequentially ground and polished using the EcoMet-300 semi-automatic grinding and polishing system (Buehler, Leinfelden-Echterdingen, Germany) with applied Kemet polycrystalline diamond suspensions (Kemika, Moscow, Russia). The thickness of the samples after mechanical treatment was 1 mm. The annealing procedure of the $\text{MgAl}_2\text{O}_4:x\text{Ce}$ ceramics was carried out by an LHT 02/18 muffle atmospheric furnace (Nabertherm, Lilienthal, Germany) at a temperature of 1300 °C for 4 h.

3.2. Experimental

Particle-size distribution analysis of the initial powders was carried out by SALD-7101 laser diffraction setup (Shimadzu, Kyoto, Japan). The powder-specific surface area was determined by the low-temperature nitrogen adsorption method using Sorbi-M setup (META, Russia). X-ray phase analysis of the powders and $\text{MgAl}_2\text{O}_4:\text{Ce}$ ceramics were conducted by XRD-7000S diffractometer (Shimadzu, Kyoto, Japan). The measurement mode was realized using CuK α radiation in the angle range from 15 to 90 degrees with a step of 0.02 degrees. The PowderCell v.2.4 software and the international crystallographic database PDF 4 were used for results interpretation.

The microstructure in oxide powders and ceramics was studied using a scanning electron microscope (JEOL JSM-7500FA, Tokyo, Japan) and a transmission electron microscope (JEOL JEM-2100F, Tokyo, Japan). The two-beam spectrophotometer SF-256UVI (Lomo-Photonics SF-256 UVI; Saint-Petersburg, Russia) was employed for optical properties measurements in the 190–1100 nm spectral range.

To excite the pulse cathodoluminescence, a handmade electron accelerator of the GIN-600 type was used. The pulse duration and average energy of accelerated electrons was 12 ns and 240 keV, respectively. The spinel ceramics were placed in a vacuum chamber. The cathodoluminescence spectra were measured using “per pulse” mode by an AvaSpec-2048 fiber optic spectrometer system (Apeldoorn, Netherlands) in spectral range from 200 to 1100 nm. The all-measured spectra were corrected for the spectral sensitivity of the optical path. The cathodoluminescence decay kinetics was recorded using an FEU-97 photomultiplier tube (Moscow, Russia) via an MDR-12 monochromator and a Tektronix DPO3034 digital oscilloscope (300 MHz)

4. Conclusions

The series of $\text{MgAl}_2\text{O}_4:\text{Ce}$ ceramics with high cerium ion concentrations were fabricated by SPS method. The characterization of the obtained oxide ceramics was aimed at evaluating the morphology, structural composition, to study the optical and spectral-luminescent properties, as well as the luminescence decay time. According to XRD analysis,

all prepared spinel ceramics were biphasic with structural impurities. The new phases of CeO₂ appeared in samples doped with Ce ions above 1 wt.%. Optical properties of MgAl₂O₄:Ce ceramics decreased from about 70% to less than 10% when the Ce concentration increased. The transparency for annealed ceramics at 1300 °C for 4 h changed significantly. There are three broad emission bands in cathodoluminescence spectra observed that correspond to intrinsic and impurities centers in spinel ceramics. The best emitting properties were recorded for a cerium concentration of 5 wt.% for annealed MgAl₂O₄:Ce ceramics. However, the optimal optical-luminescent properties were achieved for a concentration of 0.1 wt.% CeO₂ (luminescence intensity is 30% lower than the concentration of 5 wt.% CeO₂, with normal quality of transparency). The obtained dependencies of luminescent properties from the cerium concentration, temperature annealing and the SPS technological modes can be used to create efficient converters of high-energy ionizing radiation.

Author Contributions: Conceptualization, D.V., S.S., V.P., E.D. and O.K.; formal analysis, E.D., O.K. and L.C.; investigation, D.V., S.S., V.P., E.D. and L.C.; resources, O.K.; writing—original draft preparation, D.V. and S.S.; visualization, D.V. and S.S.; funding acquisition, D.V. All authors have read and agreed to the published version of the manuscript.

Funding: This work was funded by the Russian Science Foundation (Project number 21-73-10100).

Institutional Review Board Statement: Not applicable.

Informed Consent Statement: Not applicable.

Data Availability Statement: Not applicable.

Acknowledgments: Experimental measurements were carried out in CSU NMNT TPU (RF MES project #075-15-2021-710).

Conflicts of Interest: The authors declare no conflict of interest.

References

1. Rubat du Merac, M.; Kleebe, H.-J.; Müller, M.M.; Reimanis, I.E. Fifty years of research and development coming to fruition; unraveling the complex interactions during processing of transparent magnesium aluminate (MgAl₂O₄) spinel. *J. Am. Ceram. Soc.* **2013**, *96*, 3341–3365. [[CrossRef](#)]
2. Xiao, Z.; Yu, S.; Li, Y.; Ruan, S.; Kong, L.B.; Huang, Q.; Huang, Z.; Zhou, K.; Su, H.; Yao, Z.; et al. Materials development and potential applications of transparent ceramics: A review. *Mater. Sci. Eng. R Rep.* **2020**, *139*, 100518. [[CrossRef](#)]
3. Li, J.G.; Ikegami, T.; Lee, J.-H. Fabrication of translucent magnesium aluminum spinel ceramics. *J. Am. Ceram. Soc.* **2000**, *83*, 2866–2868. [[CrossRef](#)]
4. Klym, H.; Karbovnyk, I.; Piskunov, S.; Popov, A. Positron Annihilation Lifetime Spectroscopy Insight on Free Volume Conversion of Nanostructured MgAl₂O₄ Ceramics. *Nanomaterials* **2021**, *11*, 3373. [[CrossRef](#)] [[PubMed](#)]
5. Tokariev, O.; Steinbrech, R.W.; Schnetter, L.; Malzbender, J. Micro- and macro-mechanical testing of transparent MgAl₂O₄ spinel. *J. Mater. Sci.* **2012**, *47*, 4821–4826. [[CrossRef](#)]
6. Shi, Z.; Zhao, Q.; Guo, B.; Ji, T.; Wang, H. A review on processing polycrystalline magnesium aluminate spinel (MgAl₂O₄): Sintering techniques, material properties and machinability. *Mater. Design.* **2020**, *193*, 108858. [[CrossRef](#)]
7. Zhang, J.; Lu, T.; Chang, X.; Wei, N.; Xu, W. Related mechanism of transparency in MgAl₂O₄ nano-ceramics prepared by sintering under high pressure and low temperature. *J. Phys. D Appl. Phys.* **2009**, *42*, 052002. [[CrossRef](#)]
8. Wiglusz, R.J.; Boulon, G.; Guyot, Y.; Guzik, M.; Hreniak, D.; Strek, W. Structural and spectroscopic properties of Yb³⁺-doped MgAl₂O₄ nanocrystalline spinel. *Dalton Trans.* **2014**, *43*, 7752–7759. [[CrossRef](#)]
9. Kato, T.; Nakauchi, D.; Kawaguchi, N.; Yanagida, T. Thermally-stimulated luminescence and optical properties of Eu-doped MgAl₂O₄ transparent ceramics. *J. Lumin.* **2022**, *251*, 119136. [[CrossRef](#)]
10. Katsumata, T.; Minowa, S.; Sakuma, T.; Yoshida, A.; Komuro, S.; Aizawa, H. X-ray Excited Optical Luminescence from Mn Doped Spinel Crystals. *ECS Solid State Lett.* **2014**, *3*, R23–R25. [[CrossRef](#)]
11. Ramisetty, M.; Sastri, S.; Kashalikar, U.; Goldman, L.M.; Nag, N. Transparent polycrystalline cubic spinels protect and defend. *Am. Ceram. Soc. Bull.* **2013**, *92*, 20–25.
12. Goldstein, A. Correlation between MgAl₂O₄-spinel structure, processing factors and functional properties of transparent parts (progress review). *J. Eur. Ceram. Soc.* **2012**, *32*, 2869–2886. [[CrossRef](#)]
13. Alekseev, M.K.; Kulikova, G.I.; Rusin, M.Y.; Savanina, N.N.; Balabanov, S.S.; Belyaev, A.V.; Gavrishchuk, E.M.; Ivanov, A.V.; Rizakhanov, R.N. Transparent ceramics prepared from ultrapure magnesium aluminate spinel nanopowders by spark plasma sintering. *Inorg. Mater.* **2016**, *52*, 324–330. [[CrossRef](#)]

14. Ganesh, I. A review on magnesium aluminate (MgAl_2O_4) spinel: Synthesis, processing and applications. *Int. Mater. Rev.* **2013**, *58*, 63–112. [[CrossRef](#)]
15. Zou, Y.; He, D.; Wei, X.; Yu, R.; Lu, T.; Chang, X.; Wang, S.; Lei, L. Nanosintering mechanism of MgAl_2O_4 transparent ceramics under high pressure. *Mater. Chem. Phys.* **2010**, *123*, 529–533. [[CrossRef](#)]
16. Chen, Q.; Meng, C.; Lu, T.; Chang, X.; Ji, G.; Zhang, L.; Zhao, F. Enhancement of sintering ability of magnesium aluminate spinel (MgAl_2O_4) ceramic nanopowders by shock compression. *Powder Technol.* **2010**, *200*, 91–95. [[CrossRef](#)]
17. Sutorik, A.C.; Gilde, G.; Swab, J.J.; Cooper, C.; Gamble, R.; Shanholtz, E. Transparent solid solution magnesium aluminate spinel polycrystalline ceramic with the alumina-rich composition $\text{MgO}\cdot 1.2\text{Al}_2\text{O}_3$. *J. Am. Ceram. Soc.* **2012**, *95*, 636–643. [[CrossRef](#)]
18. Dericioglu, A.F.; Boccaccini, A.R.; Dlouhy, I.; Kagawa, Y. Effect of Chemical Composition on the Optical Properties and Fracture Toughness of Transparent Magnesium Aluminate Spinel Ceramics. *Mater. Trans.* **2005**, *46*, 996–1003. [[CrossRef](#)]
19. Chaim, R.; Marder, R.; Estournes, C. Optically transparent ceramics by spark plasma sintering of oxide nanoparticles. *Scr. Mater.* **2010**, *63*, 211–214. [[CrossRef](#)]
20. Jiang, D.T.; Hulbert, D.M.; Kuntz, J.D.; Anselmi-Tamburini, U.; Mukherjee, A.K. Spark plasma sintering: A high strain rate low temperature forming tool for ceramics. *Mater. Sci. Eng. A-Struct. Mater. Prop. Microstruct. Processing* **2007**, *463*, 89–93. [[CrossRef](#)]
21. Wang, C.; Zhao, Z. Transparent MgAl_2O_4 ceramic produced by spark plasma sintering. *Scr. Mater.* **2009**, *61*, 193–196. [[CrossRef](#)]
22. Frage, N.; Hulbert, D.M.; Kuntz, J.D.; Anselmi-Tamburini, U.; Mukherjee, A.K. Spark plasma sintering (SPS) of transparent magnesium-aluminate spinel. *J. Mater. Sci.* **2007**, *42*, 3273–3275. [[CrossRef](#)]
23. Lemanski, K.; Deren, P.J.; Walerczyk, W.; Strek, W.; Boulesteix, R.; Epherre, R.; Maître, A. Spectroscopic and structural properties of $\text{MgAl}_2\text{O}_4\text{:Nd}^{3+}$ nanopowders and ceramics. *J. Rare Earths* **2014**, *32*, 265–268. [[CrossRef](#)]
24. Kato, T.; Nakauchi, D.; Kawaguchi, N.; Yanagida, T. Optical, scintillation, and dosimetric properties of Dy-doped MgAl_2O_4 transparent ceramics. *Optik* **2020**, *207*, 164433. [[CrossRef](#)]
25. Raja, E.A.; Menon, S.; Dhabekar, B.; Rawat, N.S.; Gundu Rao, T.K. Investigation of defect centres responsible for TL/OSL in $\text{MgAl}_2\text{O}_4\text{:Tb}^{3+}$. *J. Lumin.* **2009**, *129*, 829–835. [[CrossRef](#)]
26. Wiglusz, R.J.; Grzyb, T.; Lukowiak, A.; Głuchowski, P.; Lis, S.; Strek, W. Comparative studies on structural and luminescent properties of $\text{Eu}^{3+}\text{:MgAl}_2\text{O}_4$ and $\text{Eu}^{3+}/\text{Na}^+\text{:MgAl}_2\text{O}_4$ nanopowders and nanoceramics. *Opt. Mat.* **2012**, *35*, 130–135. [[CrossRef](#)]
27. He, L.; Fan, G.; Lei, M.; Lou, Z.; Zheng, S.; Su, C.; Zhang, T. Preparation of $\text{MgAl}_2\text{O}_4\text{:Ce}$: YAG transparent ceramics by hot-pressed sintering and its microstructure. *Rare Met. Mater. Eng.* **2013**, *42*, 463–466.
28. Harris, D.C.; Johnson, L.F.; Seaver, R.; Lewis, T.; Turri, G.; Bass, M.A.; Zelmon, D.E.; Haynes, N. Optical and thermal properties of spinel with revised (increased) absorption at 4 top 5 μm wavelengths and comparison with sapphire. *Opt. Eng.* **2013**, *52*, 87113.
29. Maia, A.S.; Stefani, R.; Kodaira, C.A.; Felinto, M.C.F.C.; Teotonio, E.E.S.; Brito, H.F. Luminescent nanoparticles of $\text{MgAl}_2\text{O}_4\text{:Eu}$, Dy prepared by citrate sol-gel method. *Opt. Mater.* **2008**, *31*, 440–444. [[CrossRef](#)]
30. Perkins, J.M.; West, G.D.; Lewis, M.H. Analysis and spectroscopy of rare earth doped magnesium aluminate spinel. *Adv. Appl. Ceram.* **2005**, *104*, 131–134. [[CrossRef](#)]
31. Sokol, M.; Halabi, M.; Kalabukhov, S.; Frage, N. Nano-structured MgAl_2O_4 spinel consolidated by high pressure spark plasma sintering (HPSPS). *J. Eur. Ceram. Soc.* **2017**, *37*, 755–762. [[CrossRef](#)]
32. Bonnefont, G.; Fantozzi, G.; Trombert, S.; Bonneau, L. Fine-grained transparent MgAl_2O_4 spinel obtained by spark plasma sintering of commercially available nanopowders. *Ceram. Int.* **2012**, *38*, 131–140. [[CrossRef](#)]
33. Wang, Z.; Jiao, S.; Xu, Y.; Zhang, Q.; Chen YPang, G.; Feng, S. Effects of heat-treatment on photoluminescence properties of $\text{MgAl}_2\text{O}_4\text{:Eu}^{3+}$ red phosphors synthesized by a solution combustion method. *J. Lumin.* **2019**, *211*, 108–113. [[CrossRef](#)]
34. Singh, V.; Kumar Rai, V.; Watanabe, S.; Gundu Rao, T.K.; Badie, L.; Ledoux-Rak, I. Synthesis, characterization, optical absorption, luminescence and defect centers in Er^{3+} and Yb^{3+} co-doped MgAl_2O_4 phosphors. *Appl. Phys. B* **2012**, *108*, 437–446. [[CrossRef](#)]
35. Wiglusz, R.; Grzyb, T. The effect of Tb^{3+} doping on the structure and spectroscopic properties of MgAl_2O_4 nanopowders. *Opt. Mater.* **2011**, *33*, 1506–1513. [[CrossRef](#)]
36. Singh, V.; Sivaramaiah, G.; Rao, J.L.; Kim, S.H. Luminescence and electron paramagnetic resonance investigation on ultraviolet emitting Gd doped MgAl_2O_4 phosphors. *J. Lumin.* **2013**, *143*, 162–168. [[CrossRef](#)]
37. Golyeva, E.; Kolesnikov, I.; Lähderanta, E.; Kurochkin, A.; Mikhailov, M. Effect of synthesis conditions on structural, morphological and luminescence properties of $\text{MgAl}_2\text{O}_4\text{:Eu}^{3+}$ nanopowders. *J. Lumin.* **2018**, *194*, 387–393. [[CrossRef](#)]
38. Dereń, P.; Maleszka-Bagińska, K.; Głuchowski, P.; Małecka, M. Spectroscopic properties of Nd^{3+} in MgAl_2O_4 spinel nanocrystals. *J. Alloy. Compd.* **2012**, *525*, 39–43. [[CrossRef](#)]
39. Golyeva, E.; Vaishlia, E.; Kurochkin, M.; Kolesnikov, E.Y.; Lähderanta, E.; Semencha, A.; Kolesnikov, I. Nd^{3+} concentration effect on luminescent properties of MgAl_2O_4 nanopowders synthesized by modified Pechini method. *J. Solid State Chem.* **2020**, *289*, 121486. [[CrossRef](#)]
40. Balabanov, S.S.; Belyaev, A.V.; Gavrishchuk, E.M.; Mukhin, B.I.; Novikova, A.V.; Palashov, O.V.; Permin, D.A.; Snetkov, I.L. Fabrication and measurement of optical and spectral properties of the transparent Yb: MgAl_2O_4 ceramics. *Opt. Mat.* **2016**, *71*, 17–22. [[CrossRef](#)]
41. Chen, C.-F.; Doty, F.P.; Houk, R.J.T.; Loutfy, R.O.; Volz, H.; Yang, P. Characterizations of a Hot-Pressed Polycrystalline Spinel:Ce Scintillator. *J. Am. Ceram. Soc.* **2010**, *93*, 2399–2402. [[CrossRef](#)]
42. Valiev, D.; Khasanov, O.; Dvilis, E.; Stepanov, S.; Polissadova, E.; Paygin, V. Luminescent properties of MgAl_2O_4 ceramics doped with rare earth ions fabricated by spark plasma sintering technique. *Ceram. Int.* **2018**, *44*, 20768–20773. [[CrossRef](#)]

-
43. Valiev, D.; Khasanov, O.; Stepanov, S.; Dvilis, E.; Paygin, V. MgAl₂O₄ ceramics doped with rare earth ions: Synthesis and luminescent properties. *AIP Conf. Proc.* **2019**, *2174*, 020262. [[CrossRef](#)]
 44. Valiev, D.; Khasanov, O.; Stepanov, S.; Dvilis, E.; Paygin, V. Synthesis and optical properties of Tb₃₊ or Dy₃₊-doped MgAl₂O₄ transparent ceramics. *Opt. Mat.* **2019**, *91*, 396–400. [[CrossRef](#)]